



(AB)_n Segmented Copolyetherimides for 4D Printing

Minde Jin, Markus Stihl, Reiner Giesa, Christian Neuber,* and Hans-Werner Schmidt*

The fourth dimension in 4D printing comprises the ability of materials to recover their shape with time by utilizing 3D printing in combination with shape memory polymers. The focus of this work is on 3D printing of physically crosslinked thermoplastic polymers, which allow a reversible transformation from a temporary to an original shape by an external stimulus temperature, thus realize 4D printing. In this context, (AB)_n segmented copolyetherimides consisting of perylene and poly(ethylene glycol) (PEG) segments are synthesized and characterized regarding their thermal and rheological properties in view of 3D printing. The perylene imide segments act as reversible physical crosslinks which disassemble between 100 and 200 °C. The PEG segments exhibit a low melting temperature around 40 to 60 °C and are semi-crystalline at room temperature. The results show that this type of (AB)_n segmented copolyetherimide combines reliable 3D printing performance, which is indicated by low warp deformation and excellent interlayer bonding. With a blend of two copolymers, it is able to realize 4D printing.

exhibit more anisotropy due to reduced interlayer bonding quality.^[5] Printing semi-crystalline polymers with a low degree of crystallinity (e.g., polyamide 12 or polyurethane) gain reinforcement as a result of interchain crystallization at the interface. However, semi-crystalline polymers with a higher degree of crystallinity, such as polyethylene or polypropylene, exhibit detrimental material shrinkage of the printed part.^[7–15]

Smart materials are also in the focus of 3D printing as they offer distinct advantages.^[16] The combination of smart materials and 3D printing is reported in several review articles using the term “4D printing”.^[16–20] 4D printing allows a printed part to change its shape or function with time in response to stimuli such as pressure, temperature, pH, swelling/shrinking, or light.^[21] 4D printing opens

up new pathways for creating diverse shape-shifting concepts and functionalities, for example, soft robotics, drug delivery, tissue engineering, or biomedical devices.^[21,22]

3D printing of shape memory polymers (SMP) enables 4D printing. SMPs can be chemically tailored to allow sophisticated applications.^[21,23] For shape memory, a stimulus (temperature, moisture, etc.) is necessary to lead to a transformation from a temporary shape to the programmed original shape.^[24–27] Commonly the shape memory effect is thermally induced. Such materials are called thermosensitive SMPs. For the shape memory effect, three requirements are essential: i) crosslinks acting as fixation of the original shape, ii) a second type of physical crosslinks acting as defeasible fixation of the temporary shape allowing reversible switching, and iii) a certain degree of elasticity as shape recovery driving force.^[28,29]

The first type of crosslinks can be either chemically (covalent bonds) or physically (intermolecular interactions).^[24] Physical crosslinks require a polymer morphology that consists of at least two separated domains, for example, a crystalline and an amorphous phase. Another polymer morphology with physical crosslinks is present in (AB)_n segmented copolymers and thermoplastic elastomers.^[30] Here separated domains of the copolymer chain form hard segments that act as crosslinks and break or, more precisely, disassemble at an elevated temperature ($T_{\text{trans, (high)}}$). For shape switching, a second type of reversible physical crosslinking is required at a lower temperature ($T_{\text{trans, (low)}}$). This transition is necessary for the fixation of the temporary shape. The transition at $T_{\text{trans, (low)}}$ can be either crystallization or the glass transition of domains formed by the more flexible (soft) segments. Thus, by heating above $T_{\text{trans, (low)}}$, a certain elasticity is reached, and in combination with the stored inner energy, transformation from temporary shape

1. Introduction

Among 3D printing technologies, extrusion-based additive manufacturing (AM), often referred to as fused filament fabrication (FFF), fused layer manufacturing, or fused deposition modeling, is a widely used technique.^[1–3] Here AM combines a simplified thermoplastic extrusion process with computer-numerical-controlled technology enabling cost-effective layered processing of 3D printed parts. A feeding system conveys polymer filaments into a liquefier, and the molten material is deposited through a nozzle in a layer by layer fashion.^[4] Processing parameters, such as printing platform temperature, nozzle temperature, as well as nozzle path and printing speed, directly influence the performance of the final printed part.^[5] Due to the unique layered fabrication process, the successively deposited extrusion lines are fused together by thermal energy and mechanical pressure of the moving hot nozzle during printing.^[6] Compared with injection molding, FFF printed parts

Dr. M. Jin, M. Stihl, Dr. R. Giesa, Dr. C. Neuber, Prof. H.-W. Schmidt
 Macromolecular Chemistry and Bavarian Polymer Institute (BPI)
 University of Bayreuth
 Universitätsstraße 30, Bayreuth 95447, Germany
 E-mail: christian.neuber@uni-bayreuth.de;
 hans-werner.schmidt@uni-bayreuth.de

 The ORCID identification number(s) for the author(s) of this article can be found under <https://doi.org/10.1002/mame.202000473>.

© 2020 The Authors. Macromolecular Materials and Engineering published by Wiley-VCH GmbH. This is an open access article under the terms of the Creative Commons Attribution License, which permits use, distribution and reproduction in any medium, provided the original work is properly cited.

DOI: 10.1002/mame.202000473

to original shape occurs. Therefore, these domains are often called switching domains.^[29] In recent years, a rapidly increased number of publications have been reported on 3D and 4D printing materials and extrusion-based AM, utilizing thermo-plastic elastomers such as polyurethanes.^[17,21] However, such soft filament materials are a major challenge for the feeding systems of 3D printers. The low stiffness combined with high melt viscosity can cause filament buckling which impedes the 3D printing process.^[31]

In this paper, (AB)_n segmented copolyetherimides consisting of perylene and poly(ethylene glycol) (PEG) segments were synthesized to realize 3D and 4D printing for the first time with this class of copolymers. The same type of (AB)_n copolyetherimide was synthesized as anode material in all-organic polymer batteries.^[32] Similar polymers were also investigated, for example, in organic photovoltaics.^[33–36] In this work, aimed at 3D and 4D printing, perylene imide segments should act as reversible physical crosslinks disassembling at elevated temperatures ($T_{\text{trans.}(high)}$) while the PEG segments which are semi-crystalline at room temperature and melt around 50 °C ($T_{\text{trans.}(low)}$) should enable shape switching. Also, the crystallinity of PEG segments should improve the filament quality concerning feeding issues in extrusion-based 3D printing.

2. Results and Discussion

2.1. Synthesis and Thermal Characterization of (AB)_n Segmented Copolyetherimides

To provide materials for extrusion-based 3D printing with the additional feature of a shape memory effect, the polymer requires two separated transitions at different temperatures, $T_{\text{trans.}(low)}$ and $T_{\text{trans.}(high)}$. In this respect, the (AB)_n segmented copolyetherimides **1a** and **1b** (Figure 1) consist of polyethylene glycol segments which should crystallize above room temperature and of perylene bisimide segments which should form physical crosslinks via π - π interactions at higher temperatures. The copolyetherimides **1a** and **1b** were synthesized in the one-pot-melt polycondensation reaction of perylene-3,4,9,10-tetracarboxylic dianhydride with polyethylene glycol diamines of different length.

To determine the transition temperatures of copolyetherimides they were investigated by thermal and rheological methods. In Figure 2, second heating and cooling curves of **1a** and **1b** by differential scanning calorimetry (DSC) measurements are depicted. Both curves show one endothermic transition between 40 and 60 °C indicating the melting of the crystallized PEG segments. Polymer **1a** with the shorter PEG segment (2000 g mol⁻¹)

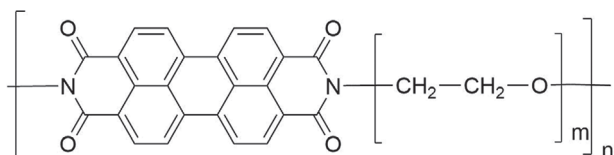


Figure 1. Chemical structure of synthesized (AB)_n segmented copolyetherimides **1a** and **1b** with rigid perylene bisimide segments and flexible polyethylene glycol (PEG) segments (**1a**: $m = 45$ (2000 g mol⁻¹), **1b**: $m = 182$ (8000 g mol⁻¹)).

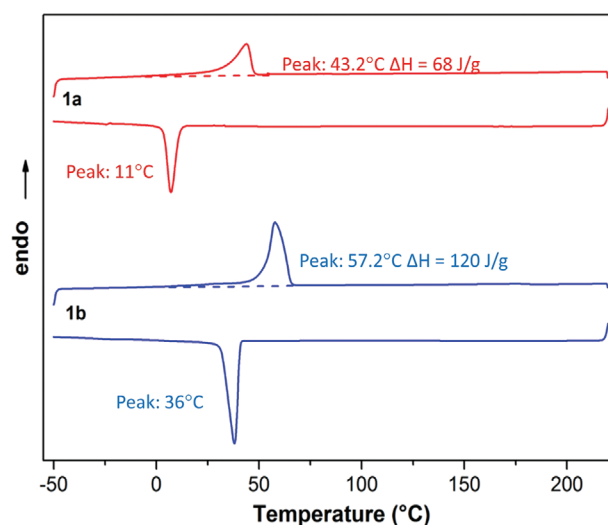


Figure 2. DSC second heating and cooling curves (rate: 10 K min⁻¹) of the (AB)_n segmented copolyetherimides **1a** and **1b** with corresponding melting temperatures and enthalpies and crystallization temperatures of the polyethylene glycol segments.

exhibits a melting peak at 43 °C with a melting enthalpy of 68 J g⁻¹. In **1b** with longer PEG segments (8000 g mol⁻¹), the crystallization is more pronounced. Here, a melting range at 57 °C with almost a doubled melt enthalpy of about 120 J g⁻¹ is measured. Both polymers show crystallization of the PEG segments with supercooling of 11 °C for **1a** and at 36 °C for **1b**. However, from the DSC measurements of **1a** and **1b** the formation of physical crosslinks by the perylene bisimide units cannot be identified at temperatures up to 220 °C. In addition, TGA measurements were carried out for **1a** and **1b** under nitrogen (Figure S1, Supporting Information). In both samples weight loss occurs above 370 °C, hence significantly higher than typically temperatures of around 200 °C used for extrusion-based AM.

Additionally, oscillator shear rheological measurements as a function of the temperature were performed (Figure 3) to investigate the formation of physical crosslinks by the perylene bisimide units. In Figure 3A and B, the storage G' (solid symbols) and the loss modulus G'' (open symbols) of **1a** and **1b** as a function of the temperature are shown. While the storage modulus G' relates to the elastic component of the system, the loss modulus G'' to the viscous component.

Consequently, if the loss modulus G'' is larger than the storage modulus G' the polymer exhibits the character of a viscous fluid. The crossing of both moduli is referred to the crossover temperature at which the viscous behavior changes to elastic behavior.^[30] For **1a**, this crossover temperature is at 65 °C, corresponding to the self-assembly of the perylene segments forming physical crosslinks. Figure 3B depicts the corresponding curves of **1b**, which contains much longer PEG segments (PEG 8000). Copolymer **1b** has a similar number of repeating units as **1a**. Here no crossover temperature is identified up the crystallization of the PEG segments. This can be explained by the lower weight fraction of perylene segments in copolymer **1b** which contains longer PEG segments. For samples **1a** and **1b**, the storage and loss moduli rapidly increases at 10 and 45 °C, which is attributed to the progressive

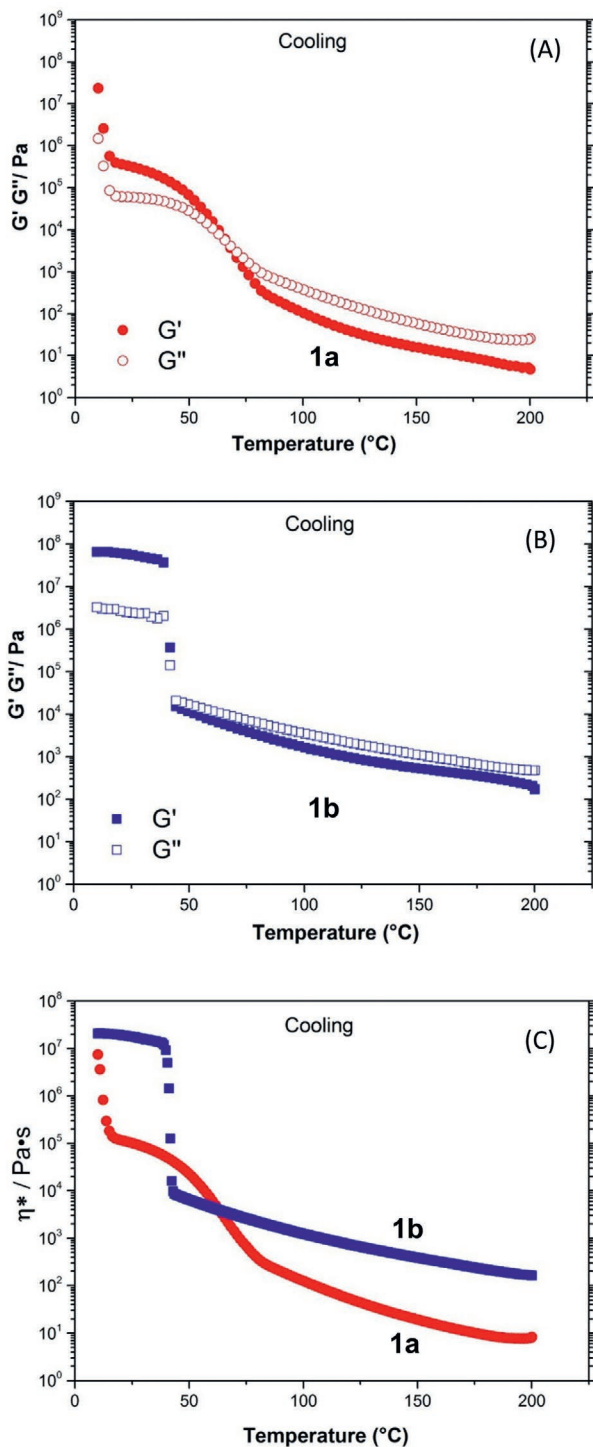


Figure 3. Oscillatory shear rheology measurements of the $(AB)_n$ segmented copolyetherimides. Storage modulus G' and loss modulus G'' of A) **1a** and B) **1b**, and C) melt viscosity of **1a** and **1b** as a function of the temperature (Plate-plate 25 mm, 0.5 Hz, cooling with 2 K min^{-1}).

crystallization of the PEG segments which is in excellent agreement with the DSC measurements (see Figure 2). In Figure 3C the complex melt viscosity plots of **1a** and **1b** upon cooling are

shown. Here both copolyetherimides **1a** and **1b** exhibit a low melt viscosity above $150 \text{ }^\circ\text{C}$ which should facilitate extrusion-based 3D printing. In contrary to **1b**, **1a** exhibits a pronounced transition at around $50\text{--}70 \text{ }^\circ\text{C}$ which is assigned to the disassembly of the perylene bisimide segments ($T_{\text{trans,high}}$). For both **1a** and **1b**, a steep increase in viscosity is observed around 10 and $40 \text{ }^\circ\text{C}$, respectively, corresponding well with the crystallization temperatures of the PEG segments as measured by DSC ($T_{\text{trans,low}}$). In conclusion, rheology investigations indicate that extrusion-based 3D printing should be possible in the temperature range between 150 and $200 \text{ }^\circ\text{C}$ since a low viscous melt is present for both copolyetherimides.

2.2. 3D Printing of $(AB)_n$ Segmented Copolyetherimides

Figure 4 illustrates the different stages of the extrusion-based AM process. Included are also the different states of the macromolecular arrangement of investigated copolyetherimides during this process. First, the filament has to be fed into the liquefier with driving wheels. Here, the filament requires a sufficient stiffness to avoid buckling and slipping between the driving wheels. This is one of the most important factors for a controlled feeding process. In this work, the essential mechanical stability/stiffness of the filaments is provided by the aggregated perylene bisimides and the crystallized PEG segments (I).

Then, the liquefier temperature has to be above the melting temperature of the PEG segments and the transition from the assembled to disassemble state of perylene bisimides segments (II), so that an extrudable melt is obtained. After extrusion through the nozzle, the polymer melt is deposited layer by layer to build up a 3D printed part. Upon cooling, the perylene bisimide segments reassembled and form the first bonding between the layers and stabilize at this point the printed part (III). The layer bonding is further improved by the

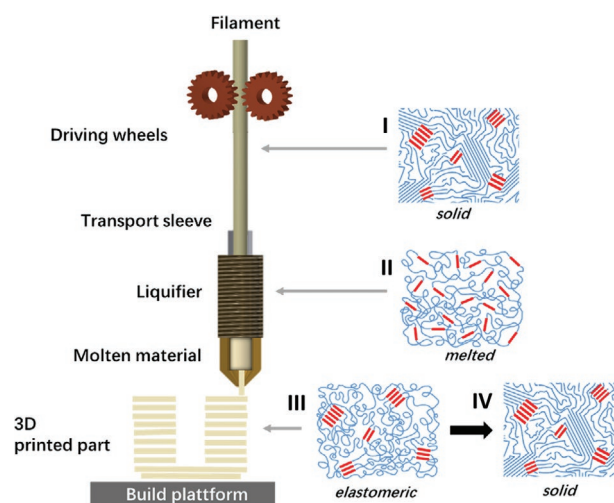


Figure 4. Schematic representation of extrusion-based additive manufacturing process and the different stages of the macromolecular arrangement (I–IV, see main text) of investigated copolyetherimides within filament feeding system (solid), liquefier (melt), and after 3D printing of the printed part (elastomeric and solid).

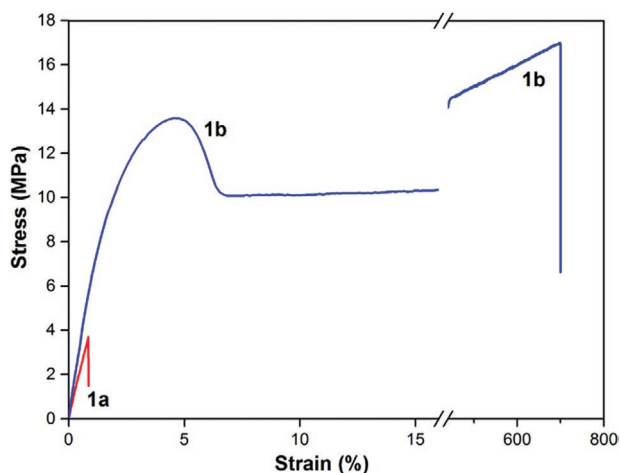


Figure 5. Stress-strain curves of injection-molded filament rods of $(AB)_n$ segmented copolyetherimides **1a** (red) and **1b** (blue). Due to the relatively short PEG 2000 segments of **1a**, it exhibits a more brittle behavior compared to **1b** possessing PEG 8000 segments.

crystallization of PEG segments at a lower temperature (IV). As mentioned above, for an efficient transport through the driving wheels and the feeding zone, the polymers require a certain filament strength and stiffness. Therefore, tensile tests of injection-molded filament rods were carried out.

2.2.1. Mechanical Characterization by Tensile Tests

Stress-strain curves of injection-molded filament rods of **1a** and **1b** are shown in **Figure 5** and the obtained data are listed in **Table 1** (see also **Figure S3**, Supporting Information). The stress-strain curves shown are one representative example of actually tested ten different specimens.

The behavior of copolyetherimides **1a** is described by an extremely brittle character with an elongation at break of only 1.5% and a stress at break of 3.8 MPa in combination with an E-modulus of 450 MPa. Thus, at room temperature, **1a** lost any elastomer properties. In contrary, copolyetherimide **1b** shows a mechanical behavior of a typical semi-crystalline polymer with a yield point, strain hardening, and ultimate strength. In **1b**, packing and crystallization of the longer PEG segments are improved and the E-Modulus is higher at about 690 MPa. The E-Moduli of **1a** and **1b** provide sufficient stiffness required for feeding in extrusion-based 3D printers.

Table 1. E-modulus (E), stress at break (σ_{br}), and elongation at break (ϵ_{br}) of injection-molded filament rods of $(AB)_n$ segmented copolyetherimides **1a** and **1b**.

Copolymer	E [MPa]	σ_{br} [MPa]	ϵ_{br} [%]
1a	454 (98) ^{a)}	3.8 (0.1)	1.5 (0.2)
1b	688 (108)	16.0 (0.3)	700 (50)

^{a)}Standard deviation in parentheses of at least ten samples. Experimental details can be found in the Experimental Section.

2.2.2. 3D Printing

The final dimensions of injection-molded filament rods are controlled by the Teflon tube inner diameter and the length of the mold. To prepare much longer pieces of one filament rod, several rods were welded together by joining two heated ends inside of a short piece of the Teflon tube. More details about this process are included in the **Figure S2**, Supporting Information. To achieve dimensional stable and defect-free 3D printed parts, processing parameters, such as liquefier and printing platform temperature, as well as cooling fan speed, have to be optimized for each polymer. Therefore, copolyetherimides **1a** and **1b** were printed first into small square tubes, these tubes were analyzed, parameters changed, and thus printing variables optimized (**Table S1**, Supporting Information). Utilizing these optimized printing parameters, **1a** and **1b** could be successfully 3D printed to U- or spiral shapes (**Figure S4**, Supporting Information). The extruded material flow was very constant during the printing process and the first printed layer adhered well on the blue tape 3D printing platform. The good quality of the printed square tubes assured reproducible mechanical testing results. **Figure 6A** demonstrates the low surface roughness and geometric deformation of a square tube using **1b**.

Due to the square tube shape, tensile specimens of different orientations to the layer deposition direction can be punched out of the sidewalls and characterized by tensile tests. For example, stress-strain curves of **1b** are plotted in **Figure 6B**. Here, the 0° specimen, which should be more similar to the properties of an extruded and injection-molded material, features a very high elongation at break of about 1400% and is therefore comparable with the tensile data measured of injection-molded filament rods (**Table 1**). More interesting is the elongation at break of the 90°-specimens reflecting the inter-layer bonding strength of printed parts. The value of 7.2% and the yield stress of 14 MPa can be considered a typical value for semi-crystalline polymers utilized for 3D printing. An option to further improve the interlayer bonding strength could be the use of copolymers with higher molecular weights.

In **Table 2**, tensile properties of copolymer **1b** investigated on injection-molded filament rods as bulk material and dogbones punched out of 3D printed square tube sidewalls are listed. The E-moduli of tensile specimens obtained by different methods range between 610 and 688 MPa and thus are comparable.

2.3. 4D Printing

The 4D printing concept is illustrated in **Figure 7** by realizing a shape memory utilizing the phase transitions of the presented $(AB)_n$ segmented copolyetherimides. First, an original U-shape is 3D printed consisting at room temperature of crystallized PEG and aggregated perylene bisimide segments. When the original shape is heated above $T_{trans.(low)}$, the polymer softens (1 – Softening) owed to the melting of the PEG segments. In this state, the U-shape can be transformed by an external force into the temporary shape (2 – External force), for example, here a V-shape. As at $T_{trans.(low)}$ the molten PEG segments are chemically attached to the aggregated perylene bisimide segments, an elastomeric behavior is present. Then, after cooling below

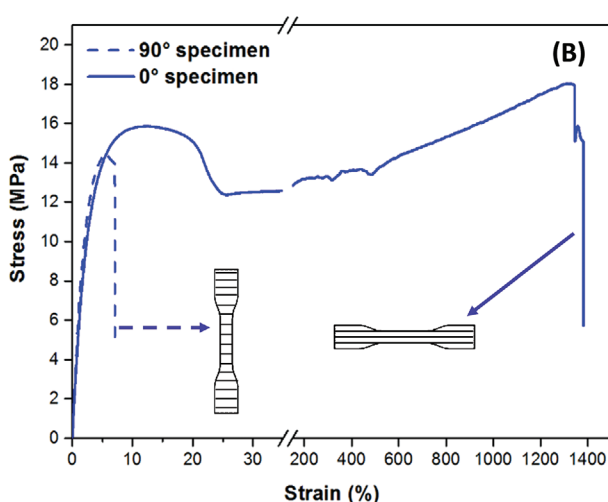
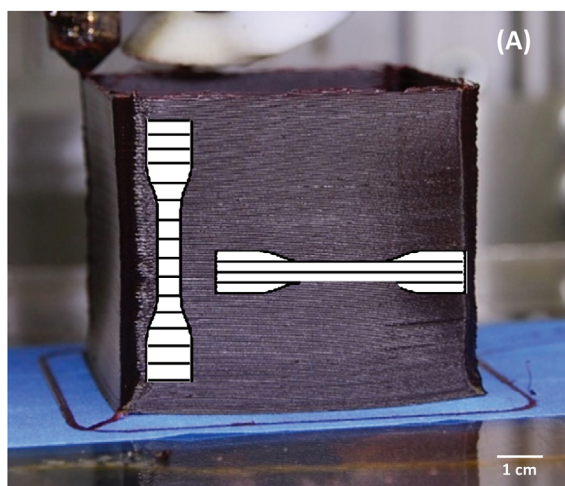


Figure 6. A) Image of a square tube obtained by extrusion-based 3D printing at 170 °C utilizing copolymer **1b**. Dogbones shown are not at scale. B) Stress-strain curves of 90° and 0° test specimens punched out of side-walls of a printed square tube with different orientation to the layer deposition direction. Samples, punched in printing direction (0°), exhibit a tensile behavior with necking and strain hardening, whereas samples punched in 90° direction are much weaker and reflect the interlayer bonding strength.

Table 2. Comparison of the mechanical properties of 3D printed parts and injection-molded rods of copolyetherimide **1b**.

Sample	E [MPa] ^{a)}	σ_{br} [MPa] ^{b)}	ϵ_{br} [%] ^{c)}
3D printed part 90° ^{d)}	644 (54) ^{e)}	14.4 (0.2)	7.2 (0.2)
3D printed part 0° ^{d)}	659 (66)	18.2 (0.2)	1400 (60)
Injection molded rod ^{f)}	688 (108)	16.0 (0.3)	700 (50)

^{a)}E-modulus; ^{b)}Stress at break; ^{c)}Elongation at break; ^{d)}Orientation of tensile loading direction to layer deposition direction of punched dogbones from 3D printed square tube; ^{e)}Standard deviation in parentheses of at least ten samples; ^{f)}See Table 1. Experimental details can be found in the Experimental Section.

$T_{trans.(low)}$, the temporary shape is fixed (3 – Fixation) and possesses long-term shape stability under ambient conditions. Heated again above $T_{trans.(low)}$ softens the polymer (4 – Softening) and allows the recovery driven by elastomeric restoring forces (5 – Shape recovery). The recovered shape is then fixed by cooling below $T_{trans.(low)}$ (6 – Fixation).

2.3.1. Blend of Copolyetherimides

For the realization of a shape memory effect using a thermoplastic polymer, two thermal transition temperatures are required. The lower thermal transition, $T_{trans.(low)}$, should be clearly above room temperature, so a fixation of a temporary shape is possible. The second thermal transition, $T_{trans.(high)}$, should be at a significantly higher temperature, so the physical crosslinks are sufficiently stable at $T_{trans.(low)}$. But DSC curves of copolyimides **1a** and **1b** (see Figure 2) exhibit only one thermal transition at around 40 and 60 °C, respectively, which are attributed to the melting of PEG crystals. No indication for an aggregation of the rigid perylene bisimide segments can be identified. However, rheological investigations (see Figure 3) show a cross-over for **1a** at 65 °C upon cooling ($T_{trans.(high)}$). This crossover indicates the formation of physical crosslinks by assembled perylene bisimides. For investigating the potential resulting shape stability, short filament rods of **1a** and **1b** were mounted free-standing in a foam block (Figure 8A).

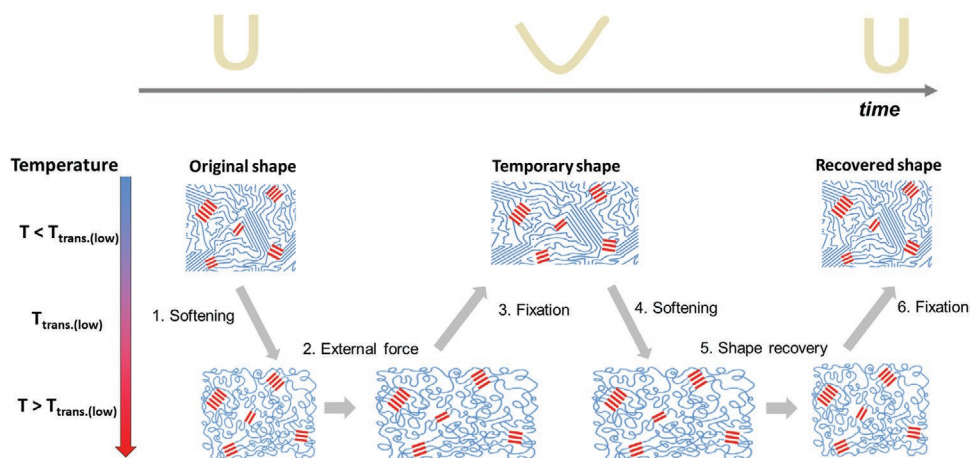


Figure 7. Schematic illustration of the transitions of using copolyetherimides when realizing the shape memory effect of a 3D printed part.

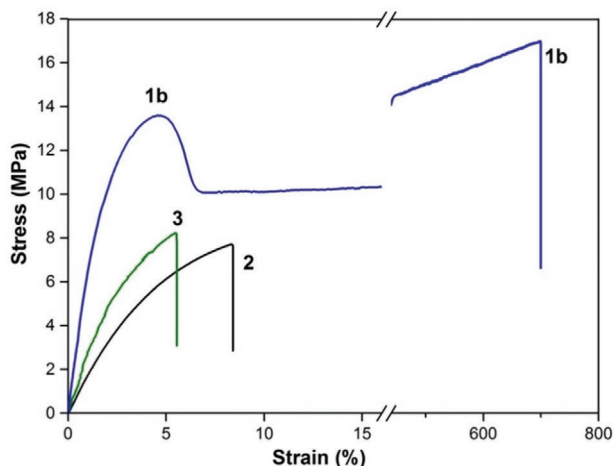


Figure 11. Stress–strain curves of filament rods of copolyetherimides **1b**, **2**, and blend **3**.

viscosity increase is less pronounced compared to **2** and turns into a plateau with a slight slope. The viscosity curves in the case of the blend **3** are a combination of both components, thus now featuring a low and a high thermal transition, $T_{\text{trans.}(low)}$ and $T_{\text{trans.}(high)}$ (see also thermal characterization by DSC Figure S5, Supporting Information). These two transitions at around 40 and 180 °C now should allow 3D printing above $T_{\text{trans.}(high)}$ and 4D printing slightly above $T_{\text{trans.}(low)}$. Also very important, each thermal transition is observed as a clear change in viscosity within a narrow temperature range.

2.3.2. 4D Printing Utilizing Blend 3

For demonstrating 4D printing, a ring-shaped self-biting snake was 3D printed in its original shape using blend **3** (Figure 14A, see also Figures S8 and S9, Supporting Information). As mentioned above, $T_{\text{trans.}(low)}$ was determined at around 40 °C; the temperature of 60 °C was selected for a shape transformation as at this temperature PEG segments are entirely melted. After heating at 60 °C for 5 min in an oven, the ring-shaped snake was transferred into the temporary shape, an open snake,

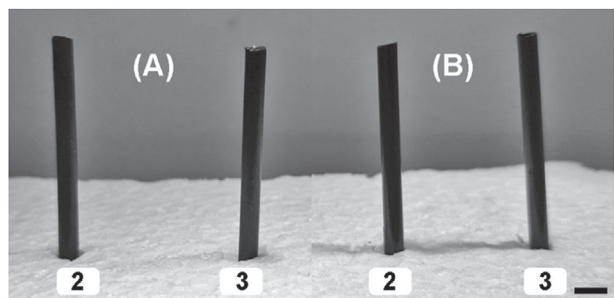


Figure 12. Demonstration of the thermal shape stability of the filament rods of copolyetherimide **2** and blend **3** (A) at room temperature and (B) after heating at 60 °C for 5 min. The aggregated perylene bisimide segments are responsible for the shape stability at 60 °C. (The scale bar represents 1 cm).

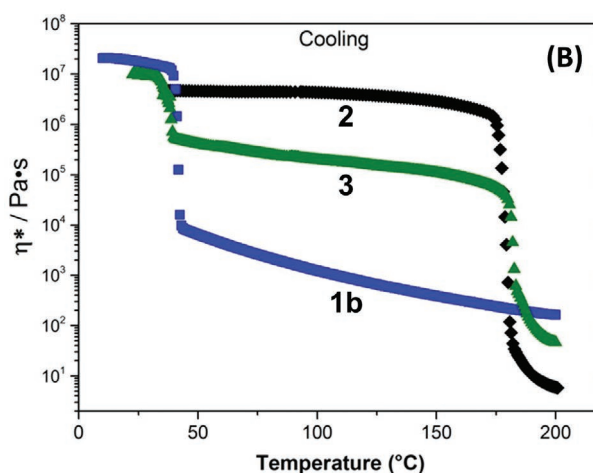
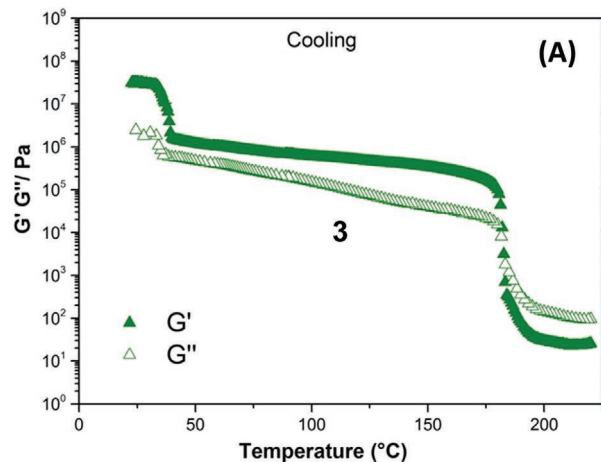


Figure 13. A) Oscillatory shear rheology measurement upon cooling of copolyetherimides blend **3**. T_{cross} in blend **3** is at 183 °C. In (B), the complex viscosity as a function of the temperature is plotted for the blend components **1b** and **2**, as well as for blend **3** itself.

and in this shape cooled down in a refrigerator to about 5 °C (Figure 14B).

By keeping the oven temperature far below $T_{\text{trans.}(high)}$ (180 °C) and due to the physical crosslinks of perylene bisimide segments, the achieved elastic deformation was fixed as open ring-shaped snake by the crystallization of the PEG segments of **1b** below 60 °C. When the temporary shape is reheated at 60 °C for 3 min, the crystallized PEG segments are melted again, the stored elastic energy is released, and the original shape recovered (Figure 14C). The printed ring-shaped snake shows an almost complete resetting of the deformation to its original shape. This shape memory was repeated several times and the recovered shape was obtained in a comparable quality.

3. Conclusion

3D and also 4D printing utilizing tailored $(AB)_n$ segmented copolyetherimides and a blend thereof is demonstrated. The copolyetherimides consist of perylene bisimide and PEG

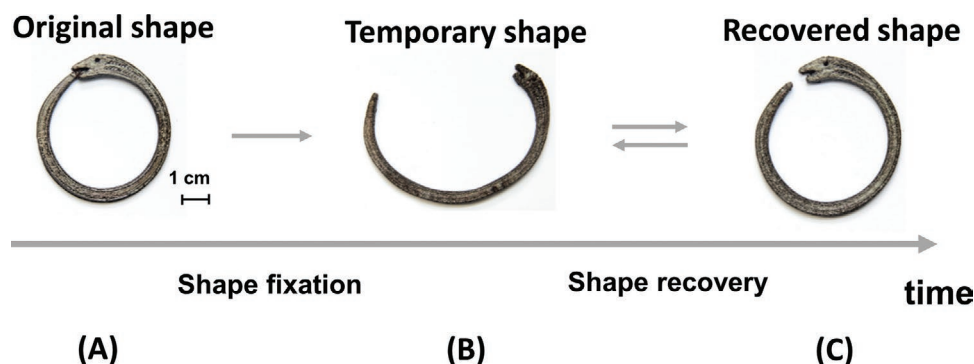


Figure 14. Demonstration of shape memory effect of a 3D printed self-biting snake. The 3D printed material is the blend **3** of copolymers **1b** and **2** in a 1:1 ratio. A) The original shape of the 3D printed object, B) the temporary shape after heating at 60 °C and cooling at 5 °C, and C) the recovered shape after reheating at 60 °C.

segments. At room temperature, the crystalline PEG segments stiffen efficiently the injection-molded filament rods and thus facilitate filament feeding utilizing a standard extrusion-based 3D printer. The necessary feature of two thermal transitions at significantly different temperatures for the realization of 4D printing was achieved by blending two different copolyetherimides. Taking advantage of the viscous melt, this blend was successfully 3D printed at 210 °C. Below the cross over temperature ($T_{\text{trans. (high)}}$) around 180 °C the π - π interactions cause the aggregation of the perylene bisimide units and prompt an elastic behavior. Finally, the reversible melting and crystallization of the PEG segments at $T_{\text{trans. (low)}}$, allowed 4D shape memory programming and shape recovering. In conclusion, the presented results demonstrate that tailored $(AB)_n$ segmented copolyetherimides feature good 3D printing performances with low warp deformation and excellent interlayer bonding strength. The prepared blend combines the two thermal transitions of each single copolyetherimide and thus provides ability of 4D printing by realizing complex geometries by established 3D printing methods.

4. Experimental Section

Materials: Polyethylene glycol diamines with molecular weights of about 2000 and 8000 g mol⁻¹ were synthesized from corresponding PEG diols via PEG-ditosylate intermediates in analogy to a known procedure.^[37,38] Jeffamine ED-900 (o,o'-bis(2-aminopropyl)polypropylene glycol-*block*-polyethylene glycol-*block*-polypropylene glycol, CAS-No: 65605-36-9) was purchased from Sigma Aldrich.^[39] The molecular weights of PEG diamines were determined by titration against 0.1 M HCl solution as Mn = 1998 g mol⁻¹ and Mn. = 7998 g mol⁻¹ for PEG diamines and as Mn = 971 g mol⁻¹ for the Jeffamine ED900. Perylene-3,4,9,10-tetracarboxylic dianhydride (CAS-No: 81-30-1) was purchased from Sigma Aldrich and used as received.

Synthesis of $(AB)_n$ Segmented Copolymers: The synthesis of the copolyetherimides **1a** and **1b** was carried out in a one-pot-melt polycondensation by reacting perylene-3,4,9,10-tetracarboxylic dianhydride with the corresponding polyethylene glycol diamine in a molar ratio of 1:1.25 (perylene: diamine). The reaction was performed at 180 °C (melt) for 24 h in a stainless-steel reactor with mechanical stirring under argon atmosphere. The completion of the reaction was confirmed with FT-IR spectroscopy. The obtained products were used without further purification. Copolyetherimide **2** with a Jeffamine ED-900 instead of the PEG segment was synthesized in the same manner.

Thermal Analysis: DSC was conducted using a Mettler Toledo DSC 2 STAR^e system under a nitrogen atmosphere from 25 to 250 °C at a heating/cooling rate of 10 K min⁻¹. Values of the melting/crystallization temperatures of the PEG segments and the disassembly/assembly temperature of perylene segments were read from the peak maximum of the second heating and cooling run, respectively.

Rheological Characterization: Oscillatory shear rheology experiments were performed on a rheometer (Kinexus lab+, Malvern Panalytical) using a 25 mm plate-plate geometry at a cooling rate of 2 K min⁻¹ and a frequency of 0.5 Hz in a temperature range from 200 to 5 °C. For the cooling run at the beginning, a constant shear strain of 0.1% was applied then switched to constant shear stress at 1000 Pa.

Lab-Scale Filament Rod Processing: The detailed preparation of lab-scale filament rods is described in a previous publication.^[12] Using a 12 mL Xplore Microinjection molder, chunks of the copolymers were melted in the barrel for ≈4 min at 200 °C for **1a** and 190 °C for **1b**. The blend **3** consisting of **1b** and **2** was prepared using a Carver 2518 hot press to mix both copolymers by compression molding of a blend **3** film, folding the film, and repeating the compression molding and folding procedure for at least ten times. The melt was then directly injected into a metal mold containing a Teflon tube with an inner diameter of 3.0 mm. Several individual filament rods obtained this way were welded together into a filament of around 90 cm length by fixating the rods in a short Teflon tube and a heat gun as heat source (see Figure S2, Supporting Information).

3D Printing: A FFF desktop 3D printer (3NTR A4, Italy) was used in this study. The nozzle diameter was 450 μm. The 3D digital models of the geometries were first designed with Autodesk Fusion 360 and additionally sliced with the software Slic3r (Version 1.3.0). For the optimization of the printing variables, a free-standing square tube of 1 × 1 cm in the base area and 1 to 5 cm in height was printed.^[12] For evaluation of printed part performance, a free-standing square tube of 5 × 5 cm base area and 5 cm in height consisting of a single line stack was 3D printed. The resulting thickness of the obtained side wall was around 750 μm. As 3D printing build surface, Scotch Blue Tape 2090 from 3M was used. To achieve dimensional stable and defect-free printed parts, each printing was optimized regarding processing parameters, such as extruder and printing platform temperature, and cooling fan speed (see Table S1, Supporting Information).

Mechanical Properties: Mechanical testing was carried out with an Instron 5565 universal tester using a 1 kN load cell and pneumatic clamps. The tensile strain was measured by a non-contacting video extensometer (AVE1). A minimum of ten specimens was measured, and the average value is reported. Short filament rods: filament rods were cut into a length of about 4 cm and tested. The E-Moduli were determined at a strain rate of 0.2 mm min⁻¹ and 0.1% and 0.3% strain. At higher strain, a rate of 10.0 mm min⁻¹ was applied until fracture of the sample. 3D printed parts: Ten test specimens with the angle of 90° and five of 0° to the layer deposition direction (X- and Y-axis) were punched out

from each sidewall of the 3D printed square tube. The E-Moduli were determined at a strain rate of 0.2 mm min⁻¹ and 0.1% and 0.3% strain. At higher strain, now a rate of 2.0 mm min⁻¹ was applied for 90° specimens and 10.0 mm min⁻¹ for the 0° specimens.

Shape Memory Testing: Shape memory experiments were conducted on 3D printed parts in form of a U-shape and a self-biting snake. A 3D digital model was designed (Autodesk Fusion 360) and additionally sliced (Slic3r Version 1.3.0) into digital layers and printed under the optimized conditions (see Table S1, Supporting Information). The original printed shape was first heated in an oven (Heraeus) at 60 °C for about 5 min to completely melt the PEG segments. At this elastic state, the shape was transferred into the temporary shape and then cooled down in a refrigerator to about 5 °C for the fixation of the temporary shape. The obtained temporary shape is long-term stable under ambient conditions. For recovery, the temporary shape was converted into the recovered shape by short-time heating at 60 °C above $T_{trans.(low)}$.

Supporting Information

Supporting Information is available from the Wiley Online Library or from the author.

Acknowledgements

The PEG diamines were kindly synthesized by Sandra Ganzleben and Jutta Failner from the Chair of Macromolecular Chemistry I, University of Bayreuth, Germany. The authors gratefully acknowledge the use of equipment in the Keylab “Small Scale Polymer Processing” of the Bavarian Polymer Institute at the University of Bayreuth.

Open access funding enabled and organized by Projekt DEAL.

Conflict of Interest

The authors declare no conflict of interest.

Keywords

3D printing, 4D printing, (AB)_n segmented copolymers, extrusion-based additive manufacturing, shape memory

Received: July 29, 2020

Revised: November 6, 2020

Published online: December 8, 2020

- [1] A. Bagsik, V. Schöppner, E. Klemp, presented at the Proc. of the 14th Int. Scientific Conf. on Polymeric Materials, Halle, Germany, September 2010.
- [2] P. Dudek, *Arch. Metall. Mater.* **2013**, *58*, 1415.
- [3] S. H. Masood, K. Mau, W. Q. Song, *Mater. Sci. Forum* **2010**, *654*, 2556.
- [4] S.-H. Ahn, M. Montero, D. Odell, S. Roundy, P. K. Wright, *Rapid Prototyping J.* **2002**, *8*, 248.
- [5] Q. Sun, G. M. Rizvi, C. T. Bellehumeur, P. Gu, *Rapid Prototyping J.* **2008**, *14*, 72.
- [6] T.-M. Wang, J.-T. Xi, Y. Jin, *Int. J. Adv. Manuf. Technol.* **2007**, *33*, 1087.

- [7] M. Spoerk, C. Holzer, J. Gonzalez-Gutierrez, *J. Appl. Polym. Sci.* **2020**, *137*, 48545.
- [8] M. Spoerk, J. Sapkota, G. Weingrill, T. Fischinger, F. Arbeiter, C. Holzer, *Macromol. Mater. Eng.* **2017**, *12*, 1700143.
- [9] O. S. Carneiro, A. F. Silva, R. Gomes, *Mater. Des.* **2015**, *83*, 768.
- [10] S. Hertle, M. Drexler, D. Drummer, *Macromol. Mater. Eng.* **2016**, *301*, 1482.
- [11] J. Z. J. Xie, *CN 201410332650*, **2014**.
- [12] M. Jin, R. Giesa, C. Neuber, H.-W. Schmidt, *Macromol. Mater. Eng.* **2018**, *303*, 1800507.
- [13] M. Jin, C. Neuber, H.-W. Schmidt, *Addit. Manuf.* **2020**, *33*, 101101.
- [14] C. G. Schirmeister, T. Hees, E. H. Licht, R. Mülhaupt, *Addit. Manuf.* **2019**, *28*, 152.
- [15] M. Spoerk, F. Arbeiter, I. Raguž, G. Weingrill, T. Fischinger, G. Traxler, S. Schuschnigg, L. Cardon, C. Holzer, *Macromol. Mater. Eng.* **2018**, *303*, 1800179.
- [16] Z. X. Khoo, J. E. M. Teoh, Y. Liu, C. K. Chua, S. Yang, J. An, K. F. Leong, W. Y. Yeong, *Virtual Phys. Prototyping* **2015**, *10*, 103.
- [17] M. D. Monzón, R. Paz, E. Pei, F. Ortega, L. A. Suárez, Z. Ortega, M. E. Alemán, T. Plucinski, N. Clow, *Int. J. Adv. Manuf. Technol.* **2017**, *89*, 1827.
- [18] S. K. Leist, J. Zhou, *Virtual Phys. Prototyping* **2016**, *11*, 249.
- [19] F. Momeni, S. M. Mehdi Hassani, N. X. Liu, J. Ni, *Mater. Des.* **2017**, *122*, 42.
- [20] J. Choi, O.-C. Kwon, W. Jo, H. J. Lee, M.-W. Moon, *3D Print. Addit. Manuf.* **2015**, *2*, 159.
- [21] C. M. González-Henríquez, M. A. Sarabia-Vallejos, J. Rodríguez-Hernández, *Prog. Polym. Sci.* **2019**, *94*, 57.
- [22] A. S. Gladman, E. A. Matsumoto, R. G. Nuzzo, L. Mahadevan, J. A. Lewis, *Nat. Mater.* **2016**, *15*, 413.
- [23] Q. Ge, A. H. Sakhaei, H. Lee, C. K. Dunn, N. X. Fang, M. L. Dunn, *Sci. Rep.* **2016**, *6*, 31110.
- [24] M. D. Hager, S. Bode, C. Weber, U. S. Schubert, *Prog. Polym. Sci.* **2015**, *3*, 49.
- [25] A. Lendlein, R. Langer, *Science* **2002**, *296*, 1673.
- [26] J. Leng, X. Lan, Y. Liu, S. Du, *Prog. Mater. Sci.* **2011**, *56*, 1077.
- [27] C. Liu, H. Qin, P. T. Mather, *J. Mater. Chem.* **2007**, *17*, 1543.
- [28] H. Tobushi, S. Hayashi, S. Kojima, *JSME Int. J., Ser. I* **1992**, *35*, 296.
- [29] D. Ratna, J. Karger-Kocsis, *J. Mater. Sci.* **2008**, *43*, 254.
- [30] G. Hochleitner, E. Fürsattel, R. Giesa, J. Groll, H.-W. Schmidt, P. D. Dalton, *Macromol. Rapid Commun.* **2018**, *39*, 1800055.
- [31] K. Elkins, K. Nordby, C. Janak, I. V. R. W. Gray, J. H. Bohn, D. G. Baird, *Solid Freeform Fabr. Symp. Proc.* **1997**, <http://hdl.handle.net/2152/71413>.
- [32] G. Hernández, N. Casado, A. M. Zamarayeva, J. K. Duey, M. Armand, A. C. Arias, D. Mecerreyes, *ACS Appl. Energy Mater.* **2018**, *1*, 7199.
- [33] Z. Liang, R. A. Cormier, A. M. Nardes, B. A. Gregg, *Synth. Met.* **2011**, *161*, 1014.
- [34] Z. Liang, R. A. Cormier, A. M. Nardes, B. A. Gregg, *MRS Online Proc. Libr.* **2011**, *10*, 1286.
- [35] E. Rostami-Tapeh-Esmail, M. Golshan, M. Salami-Kalajahi, H. Roghani-Mamaqani, *Dyes Pigm.* **2020**, *180*, 108488.
- [36] T. Sakurai, N. Orito, S. Nagano, K. Kato, M. Takata, S. Seki, *Mater. Chem. Front.* **2018**, *2*, 718.
- [37] C. Liu, J. Yuan, X. Luo, M. Chen, Z. Chen, Y. Zhao, X. Li, *Mol. Pharmaceutics* **2014**, *11*, 4258.
- [38] M. Iijima, D. Ulkoski, S. Sakuma, D. Matsukuma, N. Nishiyama, H. Otsuka, C. Scholz, *Polym. Int.* **2016**, *65*, 1132.
- [39] Huntsman Corporation, JEFFAMINE® ED-900 Polyetheramine, Technical Bulletin **2008**.